Multi-characterization of Electron-induced Defects in Highly Oriented Pyrolytic Graphite

N. Bajales[1]*, M. Ávila[2], V. Galván[1, 2], P. G. Bercoff[1, 2]*

[1] IFEG, Conicet. M. Allende s/n, Ciudad Universitaria. 5000, Córdoba. Argentina.

[1] Facultad de Matemática, Astronomía y Física, Universidad Nacional de Córdoba. M. Allende s/n, Ciudad Universitaria. 5000, Córdoba. Argentina.

* Corresponding authors.

P. G. Bercoff: Tel: +54 351 433-4051. Ext. 103. Fax: +54 351 433-4054. E-mail: bercoff@famaf.unc.edu.ar

N. Bajales: Tel: +54 351 433-4051. Int. 106. Fax: +54 351 433-4054. E-mail: bajalesluna@famaf.unc.edu.ar

Abstract

Engineering the properties of materials through defects is at the forefront of research in Materials Science. Here, we investigate the defects produced on highly oriented pyrolytic graphite (HOPG) samples irradiated with 25 keV electrons at different doses. Our samples are characterized using micro-Raman spectroscopy, small angle X-ray scattering and atomic force microscopy measurements. We assign the D mode appearance in Raman spectra to defect-like features, which induce distortions in the electronic density of HOPG after electron irradiation. These defect-like structures are interpreted in terms of a phenomenological model previously proposed by other authors. Furthermore, magnetic measurements allow to follow the changes in the magnetization of electron-irradiated HOPG. Our results show a slight increment in coercivity in irradiated samples as well as a large remanence and saturation enhancement in the sample with higher electron irradiation dose. These novel results hint that a threshold dose needs to be overcome in order to observe a magnetic response in HOPG with electron-induced defects.

Keywords: Graphite; Irradiation effect; Magnetic properties; Defects; Electron irradiation

1. Introduction

Structural disorder plays an important role in carbon-based systems from graphite to graphene[1], and has been extensively studied over the last years [2-8]. Furthermore, defect engineering is regarded as a valuable tool to harness the materials´ properties of interest in nanotechnological applications [9, 11]. The physical characteristics of carbon materials have a strong dependence on the sp^2 (graphite-like) to sp^3 (diamond-like) ratio. Different forms of sp^2-bonded carbons have various degrees of graphitic ordering, being the highly oriented pyrolytic graphite (HOPG) one of the most used as a microcrystalline carbon structure. When disorder −such as clustering of sp^2 phases, bond changes, presence of sp^2 rings, chains and sp^2/sp^3 ratio or vacancies− is introduced in the carbon matrix, the electronic and vibrational density of states are modified [12-21].

Among many suitable techniques for studying disorder in nanostructured sp^2 carbon systems, micro-Raman spectroscopy is a standard, nondestructive, rapid and likely the most sensitive tool for the characterization of crystalline, nanocrystalline and amorphous carbons. In fact, Raman spectroscopy has been used to investigate and quantify defects in carbon-based materials [22-32]. The G mode of graphite involves the in-plane motion of sp^2 C atom pairs. This mode occurs at sp^2 sites [33]. On the other hand, the D band is forbidden in perfect graphite and only becomes active when disorder is present. Its intensity, I_D, is connected to the presence of sixfold aromatic rings [2]. Tuinstra and Koenig [34] observed that the ratio of I_D to the G mode intensity, I_G, varies inversely with the diameter of the sp^2 phase clusters, L_a ($I_D/I_G \propto 1/L_a$) [34-36]. So, starting from crystalline graphite, at a fixed wavelength, the ratio I_D/I_G will increase with increasing disorder, according to Tuinstra and Koenig [34]. For small L_a, the D-mode appearance is proportional to the probability of finding a sixfold ring in the cluster, that is, proportional to the

cluster area. Likewise, the large amount of experimental visible Raman spectra could be interpreted using a phenomenological three-stage model proposed by Ferrari et al. [2], that analyzes the factors controlling the position, intensity and widths of the G and D bands. This model shows that the visible Raman spectra depend on the configuration of sp^2 sites in sp^2-bonded clusters. On the other hand, Martins Ferreira et al. [37] reported the evolution of defect-induced Raman features in carbon systems submitted to different doses of Ar-ion sputtering, from graphene to graphite. They proposed a spatial-correlation model to describe the shift in frequency and the change in linewidth of the main Raman peaks of graphene layers caused by the presence of disorder. They estimated that the typical distance between the defects, L_D, produced by Ar bombardment at different doses, is $L_D=\sigma^{-1/2}$, being σ the ion dose and assuming a homogeneous defect distribution.

An interesting phenomenon that arises from the presence of defects in carbon-based materials is the so called Defect-Induced Magnetism (DIM) [3, 4, 38-43]. Structural defects, in general, give rise to localized electronic states, a local magnetic moment, flat bands associated with defects and thus to an increase in the density of states at the Fermi level, and eventually to the development of magnetic ordering. The increasing reliability and sensitivity of impurity analysis techniques, such as particle-induced X-ray emission (PIXE) measurements at element specific absorption energies [44, 45] allowed determining the role of impurities on DIM. Magnetic measurements of HOPG and carbon films showed weak ferromagnetic signals at room temperature, observed in both pristine HOPG and after ion irradiation [46, 47]. Some authors found that ferromagnetism appears when a certain defect concentration is reached [48-51]. In fact, it has been proposed that a magnetic order exists when the density of defects in specific places is large enough, e.g. of the order of 5%, which represents an average distance between

defects of less than 2 nm [50]. Likewise, other authors showed that paramagnetism is enhanced by introducing ion-induced defects in graphite or graphene [50, 52, 53]. Moreover, magnetic moments up to 10^{-5} emu per sample were measured in thin-film-like structures generated by ion implantation in graphite [50, 51, 54]. However, there is not general consensus on the interpretation of the mechanisms that lead to the observed magnetism induced by ion irradiation. The whole subject remains controversial, especially concerning both the role of possible contamination and the mechanism responsible for the strong interaction required to lead to ferromagnetic ordering. Some observations of ferromagnetism are possibly artifacts, as described in Ref. 46, where the authors show that commonly used HOPG crystals may contain micrometer-sized magnetic particles. Recently, Y. Wang et al. [55] used neutron irradiation in HOPG to avoid the ambiguous identification of the origin of magnetism observed in ion-induced defect experiments. They showed that a large amount of defects in the bulk sample could be introduced by neutron irradiation, leading to a large measurable magnetization. First principles calculations performed by Y. Wang et al. [55] predict the formation of local magnetic moments responsible for the observed ½ spin paramagnetism. However, no ferromagnetism was reported by these authors.

In this work, we report a multi-characterization of 25 KeV electron-irradiated HOPG samples. Raman spectroscopy shows the rising and increment of the D band in irradiated samples, as well as variations in frequencies, intensities and line-widths of the G and 2D bands. We discuss these results using a phenomenological model proposed by Ferrari et al. [2]. Our analysis reveals that the noticeable vibrational modifications in HOPG could be assigned to defect-like structural distortions induced by electron-irradiation. Small-angle X-ray scattering (SAXS) and atomic force microscopy (AFM) measurements support our hypothesis of a

distortion in the electronic configuration of sp^2 orbitals due to electron bombardment. Our magnetic measurements suggest that a dose threshold should be overcome in order to induce changes in the magnetic properties of HOPG. To the best of our knowledge, this is the first time that a systematic study is carried out concerning a multi-characterization of electron irradiation experiments in HOPG. This is also the first time that an advanced characterization technique, such as SAXS, is used as a tool for investigating this type of systems.

2. Experimental details

The graphite used for this work was HOPG of ZYB grade. Three different pieces were cut from the as-received sample, into identical rectangles of 3 x 10 mm^2. Prior to any characterization, these pieces were carefully washed in acetone, to remove any possible contamination introduced during the cutting and handling [56].

Irradiation experiments were performed using an electron beam at 25 keV provided by a Jeol JXA 8230 microprobe, using two different doses: 1.7 x 10^8 e^-/cm^2 and 4.5 x 10^8 e^-/cm^2. The electron beam current was measured with a Faraday cup. In this manuscript, the sample with lower irradiation dose is referred to as Sample 1 and the one with the highest dose is Sample 2. The third piece cut from the original HOPG batch was left as a reference and is called Pristine HOPG.

In order to check for contamination, particle-induced X-ray emission (PIXE) was performed. PIXE is a useful technique for detecting magnetic contaminants, allowing the detection of magnetic elements even when the concentrations are in few parts per million. The measurements were done with a low current of protons at 2.5 MeV in order to leave fairly

undisturbed the graphite lattice previous to the electron irradiation. The 2.5 MeV protons used by PIXE provide an average chemical composition up to a depth of 57 μm from the sample surface.

Raman spectra were measured with a laser Raman spectrophotometer (Confocal Horiba Jobin-Yvon LabRam HR). The excitation wavelength and laser power were 514 nm and 2.8 ± 0.2 mW, respectively.

Small angle X-ray spectrometry (SAXS) measurements in transmission mode were performed in the SAXS1 beamline at the National Synchrotron Light Laboratory (LNLS) in Campinas, Brazil. The samples were mounted on a kapton adhesive tape in order to prevent contamination. The SAXS1 beamline works with a fixed energy of 8 keV and a beam size of 1.5 mm (horizontal) x 0.5 mm (vertical). The X-ray detection was performed with a solid state detector PILATUS 300 K with a resolution of 0.1 (δE/E). The measured q (transferred momentum) range was 0.03 $nm^{-1} < q < 1.5\ nm^{-1}$.

Atomic force microscopy (AFM) measurements were performed at room temperature using a Di-Innova Microscope (Bruker, USA) in contact mode. Standard Si cantilevers with sharp tips were used for high resolution topography imaging and the software Nanoscope Analysis was used for image analyses.

Magnetic moment measurements at 4K were performed using a superconducting quantum interference device (SQUID) magnetometer from Quantum Design with RSO. This option is appropriate to accurately measure magnetic changes in graphite samples, which are in the order of (or less than) 1 μemu [56]. In all the measurements the magnetic field was applied parallel to the graphene planes in order to diminish the contribution of the diamagnetic background. The handling of Sample 1 and Sample 2 from the irradiation chamber to the SQUID

holder was carried out using a portable vacuum chamber in order to avoid contamination during transportation.

3. Results and discussion

3.1 Raman characterization

Figure 1.a shows the Raman spectra of the two irradiated HOPG samples (Sample 1 and Sample 2) as well as the corresponding to Pristine HOPG. SEM images of the 300 µm x 160 µm irradiated areas are highlighted in Fig 1.b, where a distinctive region of higher contrast can be noticed where the electron beam was focused.

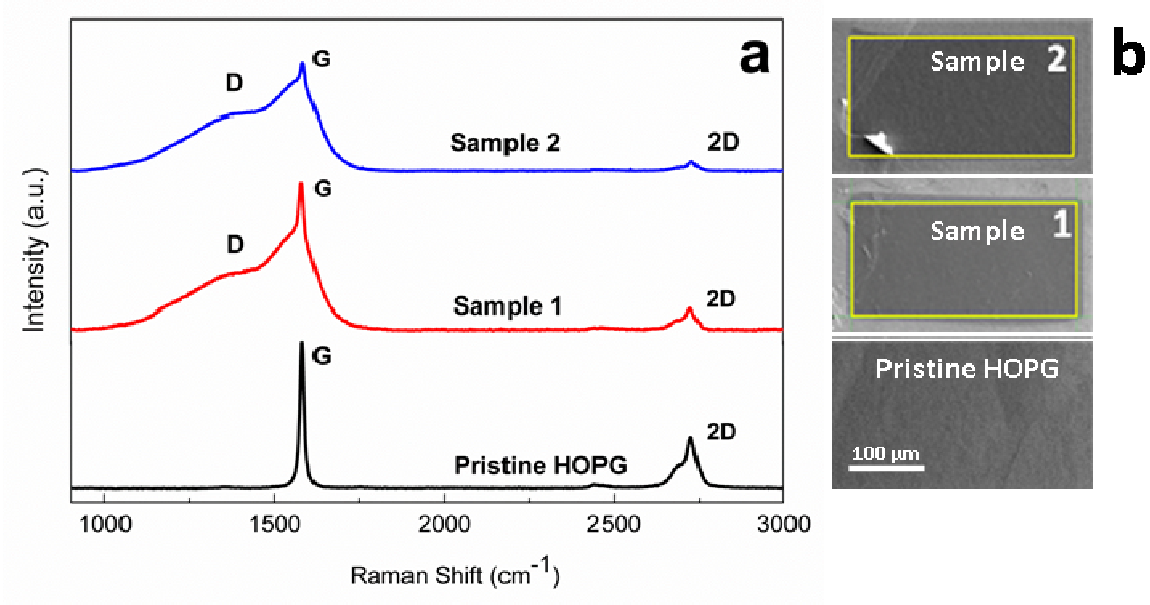

FIG. 1: a) Raman spectra of Pristine HOPG and electron irradiated HOPG samples, with increasing dose. b) SEM images of HOPG before irradiation and irradiated areas in Sample 1 and Sample 2.

The characteristic first and second order features of crystalline graphite are clearly seen in the spectra of Fig 1.a, which are normalized to the maximum, in order to stress out the changes

in the relative intensities between the G bands and the raising of D band after electron irradiation. Pristine as well as irradiated samples have the G band centered at 1580 cm^{-1} and the 2D band at 2729 cm^{-1}. The D and G bands of irradiated HOPG need three Lorentzians for a good fitting, while only two Lorentzians are required to fit the 2D band. The fitting of the experimental data is depicted in Fig. 2.a-d. Table 1 shows the peak positions and relative intensities of the corresponding components.

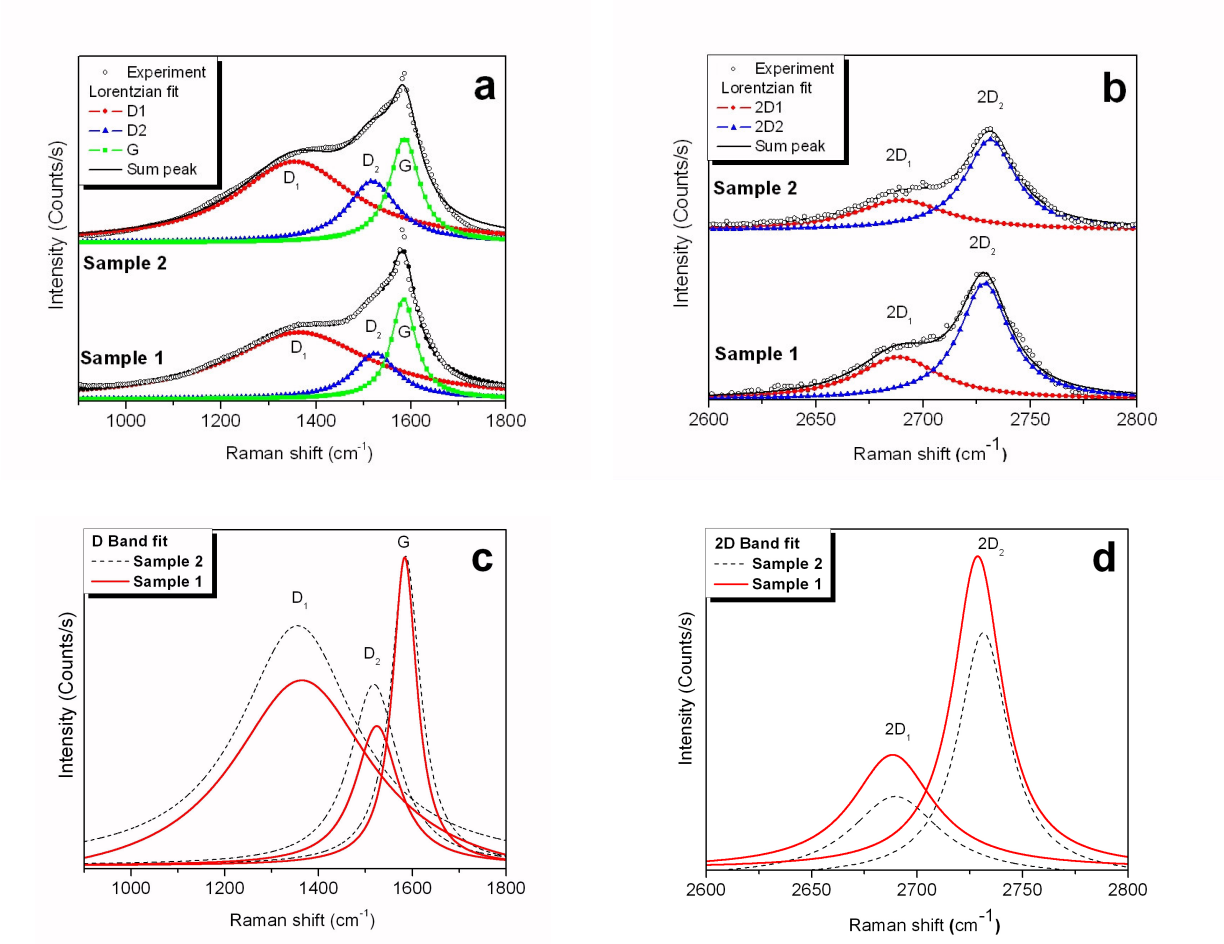

FIG. 2: D-band (a) and 2D-band (b) fittings of Sample 1 and Sample 2. Open circles indicate experimental data. Comparison between the D and 2D deconvoluted curves for both irradiated samples are shown in (c) and (d), respectively.

Table 1. Peak positions and relative intensities of bands D and 2D.

	Sample	$I_D/I_{G(fit)}$		$I_{2D}/I_{G(fit)}$	
		D1	**D2**	**2D1**	**2D2**
Frequency [cm^{-1}]	1	1360	1550	2688	2728
	2	1355	1517	2689	2731
Intensity [arb. u.]	1	0.7	0.5	0.1	0.21
	2	0.9	0.8	0.06	0.17

In Sample 1 (the sample with lower irradiation dose), we already observe the appearance of a prominent D band in the 1100 -1500 cm^{-1} range and the broadening of the G peak. The intravalley (D´) defect-induced resonant scattering process is not evident and it is not possible to resolve even with three Lorentzians. In Sample 2, we observe that the relative intensity of the D band increases as the G broadens and the 2D band decreases in intensity. Thus, the relative intensity I_D/I_G indicates that the higher the electron irradiation dose, the greater the disorder in the sp^2 network, following the same behavior reported in the literature for ion bombardment [37, 38]. In fact, with a dose of 1.7 10^8 e^-/cm^2 (Sample 1) HOPG already exhibits a significant D peak broadening, indicating strong disorder and this is more evident in the sample with highest dose (4.5 x10^8 e^-/cm^2). The decreasing intensity of the 2D peak in Sample 2 evidences the higher dose. However, we still observe some order because of the large number of untouched inner layers. 2D band is often described as simply the second order of the D feature. However, the situation is more complex since two different mechanisms are possible for the D band process (defect first and phonon second, or the other way round) while for the 2D band, only one mechanism is possible [2].

For different amorphous carbons, the D band is usually the hardest to interpret [2]. In our measurements, the observed shift of the D band to higher frequencies would suggest the presence of small aromatic clusters that contribute with higher modes. Because of the remarkable broadening of the G and D peaks, in our case it is more suitable to consider the peak areas´ ratio instead of the peak intensities´ ratio. Table 2 shows the areas' ratios A_D/A_G and A_{2D}/A_G.

Table 2. Areas' ratios of bands D and 2D.

Sample	$A_D/A_{G(exp.)}$		$A_{2D}/A_{G(exp.)}$	
	D1	**D2**	**2D1**	**2D2**
1	2.5	0.8	0.2	0.3
2	1.1	0.9	0.1	0.2

Even when the trend is the same for both peak´s and area´s ratios, the A_D/A_G and A_{2D}/A_G are better to describe the behavior of the contributions to the obtained experimental Raman spectra.

The broadening of the D peak is correlated to a distribution of sp^2 clusters with different orders and dimensions, and thus the information about the less-distorted aromatic rings is in the intensity maximum and not in the width, which depends on the disorder [2]. We do not expect defects such as hybridization changes or atom removal due to the electron beam energy. Thus, the conversion of sp^2 to sp^2/sp^3 is neglected, which means that the irradiated surface of HOPG is compatible with a nanocrystalline graphite rather than amorphous carbon. So, we could appropriately describe the electron irradiated effect as bond distortions such as angle and/or length changes.

The different types of graphitic materials can be classified according its structural order, from microcrystal to glassy carbon. The ratio sp^2/sp^3, sp^2 phase clustering, rings and chains and bonding disorder, are the factors governing the degree of graphitic ordering and the shape of the Raman spectrum. As we pointed out in the Introduction, experimental visible Raman spectra could be interpreted using a phenomenological three-stage model proposed by Ferrari et al. [2]. These authors studied the relationship between the ratio of the D and G bands intensities and the G band position as a function of the structural order in a sample. This three-stage model defines an amorphization path that goes from graphite to amorphous carbon, by studying the main effects on the evolution of the Raman spectra, described as follows:

Stage 1: From graphite to nanocrystalline graphite. The main structural change goes from a monocrystalline to a polycrystalline material with virtually no sp^3 sites. The D band appears and the ratio of intensities I_D/I_G increases. A second peak appears at 1620 cm^{-1} which merges with the G peak, resulting in a net increase of the later from 1581 to 1600 cm^{-1}.

Stage 2: From nanocrystalline graphite to amorphous carbon. Amorphous carbon arises with sp^2 bonding sites consisting of distorted sixfold rings (20% sp^3 at the most). The ratio I_D/I_G decreases with increasing amorphization. The G band becomes smooth and its position shifts from 1600 to 1510 cm^{-1}. No peaks are observed in the range 2400-3100 cm^{-1}.

Stage 3: From amorphous carbon to tetrahedral amorphous carbon. The sp^3 content rises from 20% to 85%, while the sp^2 sites change gradually from rings to chains. The ratio I_D/I_G is very low or zero. A shift of the G band position is observed from 1510 to 1570 cm^{-1}.

According to this model, the main effects observed in the evolution of the Raman spectra generated by our electron irradiation experiments agree with the first stage, being the appearance

of a D peak due to a structural change from an almost monocrystalline to a polycrystalline material. In order to have a better understanding of the electron-induced Raman spectra, we present further results concerning structural characterization by means of SAXS and AFM.

3.2 SAXS and AFM characterization

SAXS measurements are shown for the pristine and irradiated samples in Fig. 3.

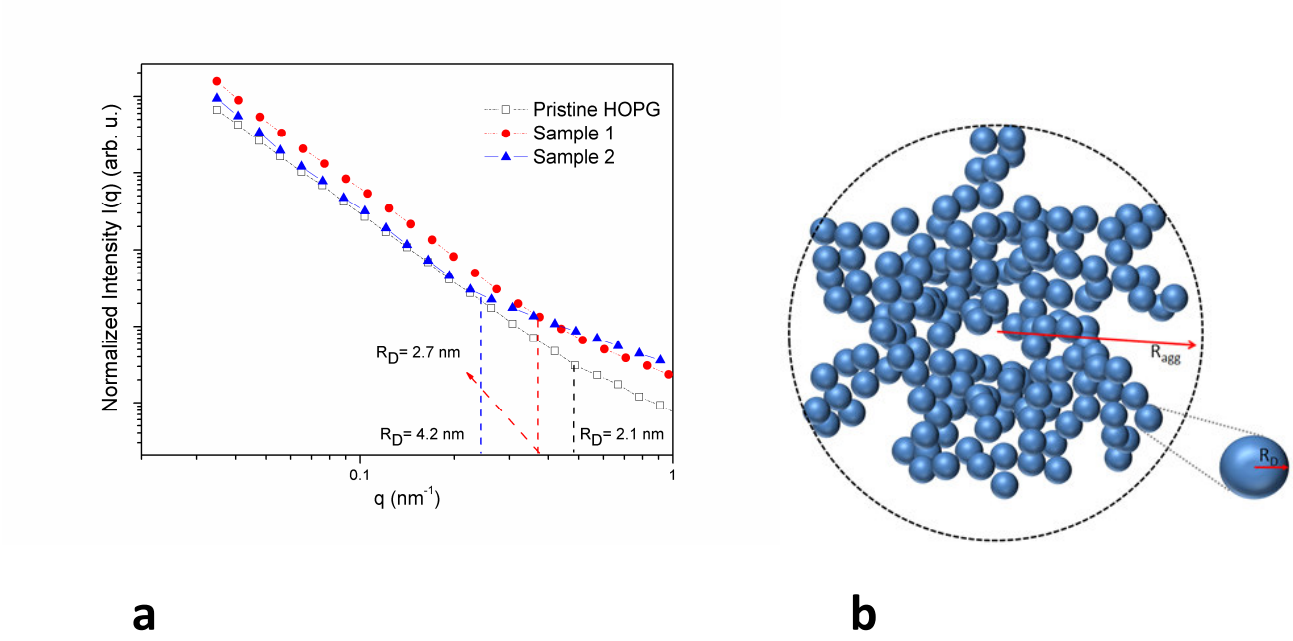

FIG. 3: a) $I(q)$ for pristine HOPG and electron irradiated samples. b) Schematic representation of the proposed fractal structure. The defect-like features generated by electron irradiation are represented by small spheres of radius R_D, which are clustered to form a 3D fractal structure of radius R_{agg}.

When going from high to intermediate q values, the change in the slope of $I(q)$ gives an idea of the mean defect size $R_D = 2\pi/q$. The parameter R_D takes into account all possible contributions

that produce electronic density fluctuations in the material, including the disorder induced by irradiation (noticed by the D-band changes in Raman spectra). For the non-irradiated sample (pristine HOPG), the characteristic defects size is related to intrinsic defects produced during manufacturing process, which are significantly lower than the ones obtained for the irradiated samples. As shown in Fig. 3.a, the parameter R_D increases with the irradiation dose.

Additional evidence of the generation of defect-like features induced by electronic irradiation is provided by AFM characterization. In fact, topographic images in Fig.4.a and 4.b show a noticeable increment of the surface roughness for Sample 2 with respect to pristine HOPG, suggesting a defect-like clustering process.

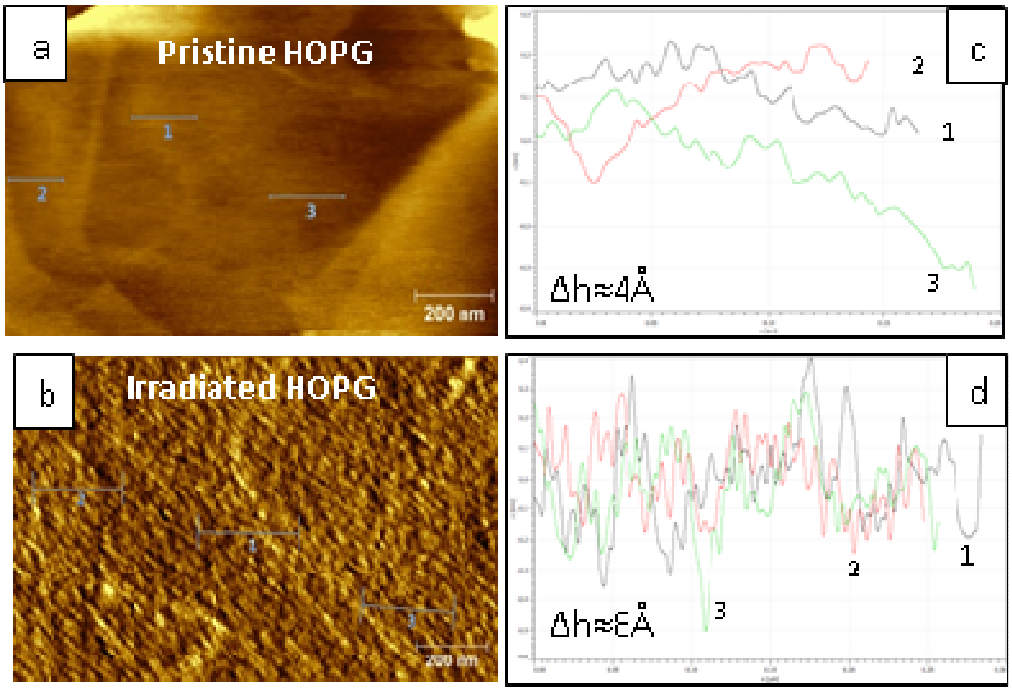

FIG. 4 AFM images of Pristine HOPG (a) and Sample 2 (b). Height profiles of pristine HOPG (c) and Sample 2 (d).

This is probably due to the fractal-like structures formation inferred from SAXS results. In addition, the flatness of the pristine HOPG is notably larger than the irradiated surface of Sample 2, evident when comparing both height profiles in Fig. 4.c and 4.d respectively. The mean roughness for Sample 2 is about 0.8 nm and the mean size of the topographic distortions is around 3 nm. Thus, according to Raman spectroscopy, AFM and SAXS results, the spatial distribution of the observed defect-like structures induced by electron-irradiation could be modelled as quasi-spherical regions of radii R_D, which are clustered to form major aggregates with characteristic size, $R_{agg,}$ (Fig. 3.b).

The mass fractal behavior gives an indication that a superstructure of defects exists (fractal). A second break in the slope of *I(q)* at very low q values should be found, located at the inverse of the typical size R_{agg} of such structures. However, in this work, q values below 0.03 nm^{-1} were not possible to explore due to experimental limitations. According to our results, we can suggest that the aggregation radius (R_{agg}) is larger than 200 nm for all samples.

As we already mentioned in the Introduction, many authors estimate the typical distance between defects (L_D) from ion irradiation, considering an homogeneous distribution of defects [37], using the relation $L_D = \sigma^{-1/2}$, where σ is the dose. If we use this expression for our experiment, a value of 100 µm as an average distance between defect-like features is obtained, which is not in agreement with our above described results. This indicates that the observed defect-like distribution induced by electron bombardment cannot be described with the same defect-distribution model as the one used for ion irradiation. However, according to Tuinstra and Koenig [34] in ion irradiation experiments, the ratio between D and G intensities (I_D/I_G) varies inversely with L_D. Moreover, the peak widths do not change considerably for low ion doses,

showing a larger increase only for L_D<4 nm (which corresponds to 6.25 10^{16} ions/cm^2) [37]. There are authors that report the D mode in disordered graphite with $L_D \approx 30$ nm [57]. In our samples, starting from disordered graphite, we observe that I_D/I_G increases with increasing disorder induced by electron irradiation, leading to a clustering process of sp^2 phases. This behavior strengthens our proposal that the structural configuration of electron-irradiated samples matches Stage 1 of the phenomenological model proposed by Ferrari et al. [2]. For more disorder, clusters of electron-induced defect-like features become smaller and more distorted, as we observed in AFM images. For small L_D, the D mode strength is proportional to the cluster area, which was estimated by means of SAXS.

In order to study the influence of the observed electronic distortions in the magnetic properties of HOPG, we discuss SQUID results in the next section.

3.3 Magnetic characterization

We performed magnetic measurements at 4K on the three studied samples to investigate if electron-irradiation is an effective method to produce DIM in HOPG. The presence of magnetic impurities in our Pristine HOPG is not apparent according to PIXE measurements (not shown), within the detection limit of this technique. However, in this sample, a hysteresis loop is observed, after subtracting the diamagnetic contribution inherent to graphite (Fig. 5). This evidences an intrinsic ferromagnetic behavior in virgin HOPG, already reported by numerous researchers in this field [46].

We find that the intrinsic ferromagnetic behavior of the pristine graphite is almost unchanged by the low-dose electron irradiation, but the remanence and saturation magnetic moment are

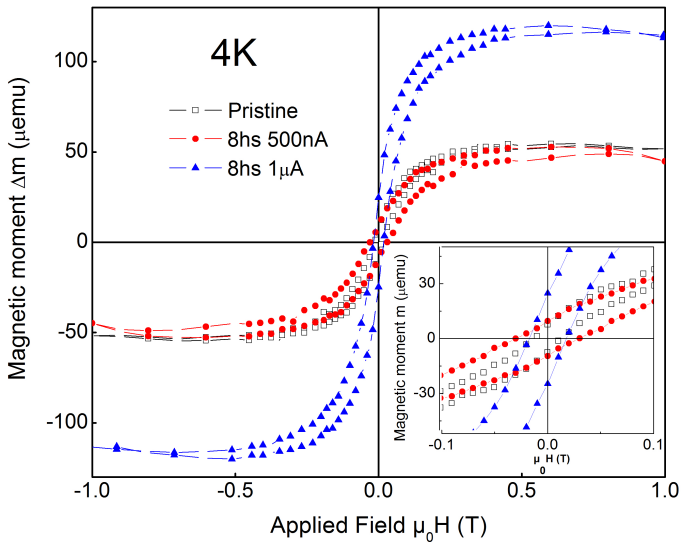

FIG. 5: Hysteresis loops of Pristine HOPG (open squares), Sample 1 (circles) and Sample 2 (triangles) after subtracting the diamagnetic background. The inset is a close-up of the low-field region, where a slight increase in coercivity and a large remanence enhancement can be noticed for Sample 2 as compared to the Pristine HOPG.

doubled in Sample 2, which was irradiated with a higher dose. There is slight coercivity increment in both, Sample 1 and 2, with respect to pristine HOPG. This effect is in agreement with some DIM experiments performed in ion-irradiated HOPG, where a threshold for the number of defects has to be overcome in order to observe a magnetic signal [48-51]. Since our electron-irradiated samples belong to the same HOPG batch as the pristine one, we state that any

changes in the magnetic behavior observed in our experiments are due to the effect of the electronic bombardment.

Further experiments are necessary in order to better understand the involved physical mechanisms that could enhance saturation and remanence in electron-irradiated HOPG, when magnetic impurities are neglected.

4. Conclusion

We show results of electronic irradiation experiments on HOPG, using a beam of 25 keV electrons at different doses. Micro-Raman spectroscopy shows strong variations in the band frequencies and line widths assigned to the D, G and 2D modes. We interpret these variations according to a phenomenological model proposed by Ferrari et al. [2], which postulates that sp^2 phase clustering processes as well as angle and length bond changes are the responsible of the D mode appearance. We assign the appearance of the D band in our samples to the distortions in the electronic density of HOPG induced by defect-like features generated after electron irradiation. We support our interpretation by means of small angle X-ray scattering and atomic force microscopy measurements, finding that the mean defect-like size is L_D=2.1 nm for the Pristine HOPG and L_D = 4.2 nm for the sample with highest irradiation dose.

The relationship between the induced distortions in the electronic density and changes in the magnetization of HOPG was also analyzed through magnetic measurements. Our results show a slight increment in coercivity in both irradiated samples as well as a large remanence and saturation enhancement in the sample with higher electron irradiation dose. Thus, any changes in the magnetic behavior of pristine HOPG are related to the probability of having a finite magnetic

moment in the irradiated samples because of a new electronic distribution around the electrons near the corresponding defect-like features.

Our results contribute to the current trend and effort in the Materials Science community to control the properties of carbon-based systems by defect engineering.

Acknowledgements

This work was financed by CONICET, FONCYT and SECyT-UNC. The authors acknowledge the Brazilian Synchrotron Light Laboratory (LNLS) for beamtime at SAXS-2.

References

[1] K. S. Novoselov, A. K. Geim, S. V. Morosov, D. Jiang, Y. Zhang, S. V. Dubonos, et al., Electric Field Effect in Atomically Thin Carbon Films, Science 2004, 306, 666-669.

[2] A. C. Ferrari and J. Robertson, Interpretation of Raman Spectra of Disordered and Amorphous Carbon, Phys. Rev. B 2000, 61, 14095-14107; doi: 10.1103/PhysRevB.61.14095.

[3] Oleg V. Yazyev, Magnetism in Disordered Graphene and Irradiated Graphite, Phys. Rev. Lett. 2008,101, 037203:1-4; doi:10.1103/PhysRevLett.101.037203.

[4] O. V. Yazyev, Emergence of Magnetism in Graphene Materials and Nanostructures, Rep. Prog. Phys. 2010, 73, 056501:1-18; doi:10.1088/0034-4885/73/5/056501.

[5] P. Araujo, M. Terrones, M. S. Dresselhaus, Defects and Impurities in Graphene-like Materials, Materials Today 2012,15, 98-109; doi: 10.1016/S1369-7021(12)70045-7.

[6] Jian-Hao Chen, W. G. Cullen, C. Jang, M. S. Fuhrer, E. D. Williams, Defect Scattering in Graphene, Phys. Rev. Lett. 2009, 102, 236805:1-4; doi:10.1103/PhysRevLett.102.236805.

[7] V. Dal Lago and L. E. F. Foa Torres, Line Defects and Quantum Hall Plateaus in Graphene, J. Phys.: Cond. Matter 2015, 27, 145303-145311; doi:10.1088/0953-8984/27/14/145303.

[8] L. E. F. Foa Torres, S. Roche and J.-C. Charlier, Introduction to Graphene-Based Nanomaterials: From Electronic Structure to Quantum Transport, Cambridge University Press: Cambridge, U.K., 2014.

[9] A.V. Krasheninnikov and F. Banhart, Engineering of Nanostructured Carbon Materials with Electron or Ion Beams, Nature Materials 2007, 6, 723-733; doi: 10.1038/nmat1996.

[10] A. Krasheninnikov, K. Nordlund, Ion and Electron Irradiation-induced Effects in Nanostructured Materials, J. Appl. Phys. 2010, 107 (7), 071301:1-70 ; doi:10.1063/1.3318261.

[11] Böttcher, D. Löffler, N. Bajales, S. Ulas, R. Machatschek, S. Malik, P. Brenner and M. M. Kappes, Nanostrutured Arrays of Stacked Graphene Sheets, Nanotechnology 2012, 23, 415302:1-13; doi: 10.1088/0957-4484/23/41/415302.

[12] N. Wada, P. J. Gaczi, A. Solin, Diamond-like' 3-fold Coordinated Amorphous Carbon, J. Non-Cryst. Solids 1980, 35 - 36, 543-548.

[13] S. R. Salis, D. J. Gardiner, M. Bowden, J. Savage, D. Rodway, Monitoring the Quality of Diamond Films using Raman Spectra Excited at 514.5 nm and 633 nm, Diamond Relat. Mater 1996, 5, 589-591 (); doi: 10.1016/0925-9635(96)90031-X.

[14] F. Li. and J. S. Lannin, Disorder Induced Raman Scattering of Nanocrystalline Carbon, Appl. Phys. Lett. 1992, 61, 2116; doi:10.1063/1.108324.

[15] G. P. Lopinski, V. I. Merkulov, J. S. Lannin, Vibrational States of Tetrahedral Amorphous Carbon, Appl. Phys. Lett. 1996, 69, 3348; doi:10.1063/1.117302.

[16] E. M. Bringa, R. E. Johnson, M. Jakas, Molecular-dynamics Simulations of Electronic Sputtering, Phys. Rev. B 1999, 60, 15107–15116.

[17] D. Schwen, E. Bringa, J. Krauser, A. Weidinger, C. Trautmann, H. Hofsass, Nano-hillock Formation in Diamond-like Carbon Induced by Swift Heavy Projectiles in the Electronic Stopping Regime: Experiments and Atomistic Simulations, Appl. Phys. Lett. 2012, 101, 113115; doi: 10.1063/1.4752455.

[18] D. Schwen, E. Bringa, Atomistic Simulations of Swift Ion Tracks in Diamond and Graphite, Nucl. Instr. Meth. Phys. Res. B 2007,256 (1), 187–192; doi: 10.1016/j.nimb.2006.12.001.

[19] N. Bajales, L. Cristina, S. Mendoza, R. Baragiola, E. Goldberg, J. Ferrón, Exciton Autoionization in Ion Induced Electron Emission, Phys. Rev. Lett. 2008, 100, 227604:1-7; doi: 10.1103/PhysRevLett.100.227604.

[20] N. Bajales, F. Bonetto, R. Vidal, E. Goldberg, J. Ferrón, Low Energy Ion Scattering in He^+/HOPG System, J. of Mol. Catal. A: Chemical- MOLCA A 2008, 281, 237-240; doi:10.1016/j.molcata.2007.10.025.

[21] J. Ferrón, R. Vidal, N. Bajales, L. Cristina , R. Baragiola , Role of HOPG Density of Empty Electronic States Above Vacuum on Electron Emission Spectra Induced by Ions and UV photons, Surf. Sci. 2014, 622, 83-86; doi:10.1016/j.susc.2013.12.010.

[22] J. Schwan, S. Ulrich, V. Bathori, H. Erhardt, S. R. P. Silva, Raman Spectroscopy on Amorphous Carbon Films J. Appl. Phys. 1996, 80, 440-447; doi:10.1063/1.362745.

[23] K. W. R. Gilkes, H. S. Sands, D. N. Batchelder, J. Robertson, W. I. Milne, Direct Observation of sp(3) Bonding in Tetrahedral Amorphous-carbon using Ultraviolet Raman-Spectroscopy, Appl. Phys. Lett. 1997, 70, 1980-1982.

[24] V. I. Merkulov, J. S. Lannin, C. H. Munro, S. A. Asher, V. S. Veerasamy, W. I. Milne, UV Studies of Tetrahedral Bonding in Diamondlike Amorphous Carbon, Phys. Rev. Lett. 1997, 78, 4869-4872; doi:10.1103/PhysRevLett.78.4869.

[25] J. Robertson and E. P. O'Reilly, Electronic and Atomic Structure of Amorphous Carbon, Phys. Rev. B 1987, 35, 2946-2957; J. Robertson, Amorphous carbon, Adv. Phys. 1986, 35, 317-374.

[26] W. A. Harrison, Bond-orbital Model and the Properties of Tetrahedrally Coordinated Solids, Phys. Rev. B 1973, 8, 4487-4498.

[27] C. A. Coulson and H. C. Longuet-Higgins, Proc. R. Soc. London, Ser. A 1947,191, 39; 1948,193, 447-464.

[28] J. Robertson, Structural Models of a-C and a-C:H, Diamond Relat. Mater. 1995, 4, 297-301.

[29] C. Mapelli, C. Castiglioni, G. Zerbi, K. Mullen, Common Force Field for Graphite and Polycyclic Aromatic Hydrocarbons, Phys. Rev. B 1999, 60, 12 710- 12 725; doi:10.1103/PhysRevB.60.12710.

[30] M. V. Bracamonte, G. I. Lacconi, S. E. Urreta, L. E. F. Foa Torres, On the Nature of Defects in Liquid-Phase Exfoliated Graphene, J. of Phys. Chem. C 2014, doi: 10.1021/jp501930a.

[31] A. Jorio, R. Saito, G. Dresselhaus, M. S. Dresselhaus, Front Matter, in Raman Spectroscopy in Graphene Related Systems, Wiley-VCH Verlag GmbH & Co. KGaA, Weinheim, Germany, 2011; doi: 10.1002/9783527632695.fmatter.

[32] A.C. Ferrari and D. M. Basko, Raman Spectroscopy as a Versatile Tool for Studying the Properties of Graphene, Nature Nanotechnology 2013, 8, 235-246; doi:10.1038/nnano.2013.46.

[33] D. Lin-Vien, N. B. Colthurp, W. G. Fateley, J. G. Grasselli, The Handbook of Infrared and Raman Characteristic Frequencies of Organic Molecules , Academic, New York, 1991.

[34] F. Tuinstra and J. L. Koening, Raman Spectrum of Graphite, J. Chem. Phys. 1970, 53, 1126-1130; doi: 10.1063/1.1674108.

[35] D. S. Knight and W. B. White, Characterization of Diamond Films by Raman Spectroscopy, J. Mater. Res. 1989, 4, 385- 393; doi: 10.1557/JMR.1989.0385.

[36] M. J. Matthews, M. A. Pimenta, G. Dresselhaus, M. S. Dresselhaus, M. Endo, Origin of Dispersive Effects of the Raman D band in Carbon Materials, Phys. Rev. B 1999, 59, 6585-6588; doi:10.1103/PhysRevB.59.R6585.

[37] E. H. Martins Ferreira, M. V. O. Mouthino, F. Stavale, M. M. Lucchese, R. B. Capaz, C. A. Achete, et al., Evolution of the Raman Spectra from Single-, Few-, and Many-layer Graphene with Increasing Disorder, Phys. Rev. B 2010, 82, 125429:1-9; doi: 10.1103/PhysRevB.82.125429.

[38] T. Makarova, K.-H. Han, P. Esquinazi, R. da Silva, Y. Kopelevich, I. Zakharova, et al., Magnetism in Photopolymerized Fullerenes, Carbon 2003, 41, 1575-1584, doi: 10.1016/S0008-6223(03)00082-4.

[39] K. H. Han, D. Spemann, R. Hoehne, A. Setzer, T. Makarova, P. Esquinazi, et al., Observation of Intrinsic Magnetic Domains in C60 polymer, Carbon 2003, 41, 785-795, doi:10.1016/S0008-6223(02)00401-3.

[40] K.-H. Han, A. Talyzin, A. Dzwilewski, T. L. Makarova, R. Hohne, P. Esquinazi, et al., Magnetic Properties of Carbon Phases Synthesized using High-pressure High-temperature Treatment, Phys. Rev. B 2005, 72, 224424- 224449, doi:10.1103/PhysRevB.72.224424.

[41] S. Mathew, B. Satpati, B. Joseph, B. N. Dev, R. Nirmala, S. K. Malik, et al., Magnetism in C60 Films Induced by Proton Irradiation, Phys. Rev. B 2007, 75, 075426- 075432, doi:10.1103/PhysRevB.75.075426.

[42] R. Hoehne, P. Esquinazi, V. Heera, H. Weishart, Magnetic Properties of Ion-implanted Diamond, Diam. Relat. Mater. 2007 16, 1589 -1596, doi:10.1016/j.diamond.2007.01.019.

[43] Y. W. Ma, Y. H. Lu, J. B. Yi, Y. P. Feng, T. S. Herng, X. Liu, et al., Room Temperature Ferromagnetism in Teflon due to Carbon Dangling Bonds, Nat. Commun. 2012, 3, 727-738, doi: 10.1038/ncomms1689.

[44] H. Ohldag, P. Esquinazi, E. Arenholz, D. Spemann, M. Rothermel, A. Setzer, et al., The Role of Hydrogen in Room-temperature Ferromagnetism at Graphite Surfaces, N. J. of Phys. 2010, 12, 123012:1-10, doi:10.1088/1367-2630/12/12/123012.

[45] Y. Kopelevich, P. Esquinazi, J. Torres, S. Moehlecke, Ferromagnetic- and Superconducting-Like Behavior of Graphite, J. Low Temp. Phys. 2000, 119, 691–702, doi:10.1023/A:1004637814008.

[46] M. Sepioni, R. R. Nair, I.-Ling Tsai, A. K. Geim, I. V. Grigorieva, Revealing Common Artifacts due to Ferromagnetic Inclusions in Highly-oriented Pyrolytic Graphite, EPL 2012, 97, 47001:1-8, doi:10.1209/0295-5075/97/47001.

[47] P. Esquinazi, D. Spemann, R. Hoehne, A. Setzer, K.-H. Han, T. Butz, Induced Magnetic Ordering by Proton Irradiation in Graphite, Phys. Rev. Lett. 2003, 91, 227201:1-4, doi:10.1103/PhysRevLett.91.227201.

[48] S. Zhou, E. Cizmar, K. Potzger, M. Krause, G. Talut, M. Helm, et al., Origin of Magnetic Moments in Defective TiO2 single Crystals, Phys. Rev. B 2009, 79, 113201, doi: 10.1103/PhysRevB.79.113201.

[49] Y. Liu, G. Wang, S. Wang, J. Yang, L. Chen, X. Qin, et al., Defect-Induced Magnetism in Neutron Irradiated 6H-SiC Single Crystals, Phys. Rev. Lett. 2011, 106, 087205:1-4, doi:10.1103/PhysRevLett.106.087205.

[50] M. A. Ramos, J. Barzola-Quiquia, P. Esquinazi, A. Munioz-Martin, A. Climent-Font, M. Garcia-Hernandez, Magnetic Properties of Graphite Irradiated with MeV ions, Phys. Rev. B 2010, 81, 214404:1-16, doi:10.1103/PhysRevB.81.214404.

[51] Z. He, X. Yang, H. Xia, T. Z. Regier, D. K. Chevrier, X. Zhou, et al., Role of Defect Electronic States in the Ferromagnetism in Graphite, Phys. Rev. B 2012, 85, 144406, doi:10.1103/PhysRevB.85.144406 .

[52] A. Ney, P. Papakonstantinou, A. Kumar, N.-G. Shang, N. Peng, Irradiation Enhanced Paramagnetism on Graphene Nanoflakes, Appl. Phys. Lett. 2011, 99, 102504:1-3, doi:10.1063/1.3628245.

[53] R. Nair, M. Sepioni, I.-L. Tsai, O. Lehtinen, J. Keinonen, A. Krasheninnikov, et al., Spin-half Paramagnetism in Graphene Induced by Point Defects, Nat. Phys. 2012, 8, 199-202, doi:10.1038/nphys2183.

[54] M. Roever, J. Malindretos, A. Bedoya-Pinto, A. Rizzi, C. Rauch, F. Tuomisto, Tracking Defect-induced Ferromagnetism in GaN:Gd, Phys. Rev. B 2011, 84, 081201:1-4, doi: 10.1103/PhysRevB.84.081201.

[55] Y. Wang, P. Pochet, C. A. Jenkins, E. Arenholz, G. Bukalis, S. Gemming, et al., Defect-induced Magnetism in Graphite Through Neutron Irradiation, Phys. Rev. B 2014, 90, 214435:1-10, doi:10.1103/PhysRevB.90.214435 .

[56] P. Esquinazi, J. Barzola-Quiquia, D. Spemann, M. Rothermel, H. Ohldag, N. García, et al., Magnetic Order in Graphite: Experimental Evidence, Intrinsic and Extrinsic Difficulties, J. Magn. Mag. Mat. 2010, 322 (9-12), 1156-1161, doi: 10. 1016/j.jmmm.2009.06.038.

[57] P. Lespade, A. Marchad, M. Couzi, F. Cruege, Caracterisation de Materiaux Carbones par Microspectrometrie Raman, Carbon 1984, 22, 375-385, doi:10.1016/0008-6223(84)90009-5.